Journal of Energy Storage 72 (2023) 108244

Contents lists available at ScienceDirect

Journal of Energy Storage

journal homepage: www.elsevier.com/locate/est

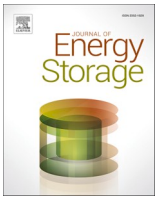

Research papers

Thin-film Li_3InCl_6 electrolyte prepared by solution casting method for all-solid-state batteries

Han-xin Mei [a], Paolo Piccardo [a,*], Giovanni Carraro [b], Marco Smerieri [b], Roberto Spotorno [a]

[a] Department of Chemistry and Industrial Chemistry, University of Genoa, Via Dodecaneso 31, 16146 Genoa, GE, Italy
[b] IMEM–CNR, via Dodecanese 32, 16146 Genoa, GE, Italy

ARTICLE INFO

Keywords:
All-solid-state battery
Thin-film solid-state electrolyte
Solution casting
Li_3InCl_6

ABSTRACT

All-solid-state batteries (ASSBs) with solid-state electrolytes (SSEs) have become a hot research topic in recent years due to their high energy density and safety. However, most research is limited to the use of electrode and electrolyte powders pressed together for testing purposes, and it is impossible to achieve the goal of mass production by manufacturing complete batteries only via compression. Such a method might need extremely high pressure to obtain a fully dense system composed of both electrodes separated by the electrolyte and the largest the battery surface the highest the pressure demanded. Therefore, how to achieve mass production of SSEs while maintaining quality control is the focus of current research. In this work, we selected Li_3InCl_6 (LIC) as a solid-state electrolyte added with a small amount of ethyl cellulose as the binder. A wet method was developed accordingly using acetonitrile as solvent to fabricate thin LIC composite film SSE (LIC-ACE) directly on filter membrane deposition. The prepared SSEs showed the following characteristics: easy to peel off from the deposition support while maintaining structural integrity, and a high ionic conductivity of 0.76 mS cm^{-1} at room temperature. The structure, porosity and other properties were determined by SEM, XRD, and BET characterization. Finally, it can withstand more than 1000 h cycles without short circuit in symmetrical Li—Li cell test and shows good electrochemical performance in the ASSBs test.

1. Introduction

Thanks to the growing awareness of the problems associated with exhaust emissions from conventional fuel vehicles, measures to protect the environment are increasingly being studied [1]. Most countries have agreed to phase out the sale of petrol vehicles after 2030, while hydrogen vehicles are still difficult to deploy on a large scale due to safety and the cost of hydrogen storage [2]. Therefore, electric vehicles, with their unique environmental friendliness and cost efficiency, are the most promising alternative to fuel-powered vehicles in the future [3]. However, the conventional lithium-ion batteries used in electric vehicles cannot yet meet the performance requirements of customers. Most models still have a range of less than 600 km and are prone to electrolyte leakage and the risk of fire in the event of a collision [4,5]. However, ASSBs have a higher energy density and lower safety risk than conventional lithium-ion batteries, so they have become a hot research topic and represent the development direction for the next generation of lithium-ion batteries [6,7].

Common SSEs can be classified into three main types depending on their composition: oxides, sulfides and polymers. Oxides have the lowest production requirements but are not flexible and are difficult to bond with electrode materials; sulfides have the highest ionic conductivity but require stringent production conditions and raw materials [8]; polymers are flexible and can form good surface contact with electrode materials but usually have low ionic conductivity at room temperature [9]. Different types of electrolytes have their properties, so composite electrolytes formed from a variety of different types of electrolytes often perform better, but sometimes pose compatibility problems and make synthesis more difficult [10].

Although halide solid-state electrolytes (HSSEs) have only come into the focus of researchers since 2018 [11], they have good prospects for application as they combine the properties of different electrolytes, can be easily synthesized by ball milling, have high ionic conductivity at room temperature, are cost-efficient, and have some flexibility and air stability [12]. Moreover, some of the HSSEs can be synthesized on a large scale by the liquid-phase method, and the whole synthesis process only needs to be carried out under an inert gas atmosphere and below 400 °C [13,14].

* Corresponding author.
E-mail address: paolo.piccardo@unige.it (P. Piccardo).

https://doi.org/10.1016/j.est.2023.108244
Received 23 March 2023; Received in revised form 7 June 2023; Accepted 30 June 2023
Available online 6 July 2023

Since most SSEs test require the use of pellets, which must be prepared by at least three powder pressings, the process is lengthy and difficult to manage [15]. Inspired by the electrode slurry and liquid phase deposition methods, we have improved the solution casting method by mixing LIC, binder, solvent and other components into a slurry and pouring it onto the surface of the filter membrane to produce LIC-ACE films. The resulting samples can be easily peeled from the filter membrane with tweezers, do not break when bent, and show good resistance to humidity. They also have a high lithium ion conductivity of 0.76 mS cm^{-1} at room temperature and show good electrochemical performance in symmetrical cells and ASSBs. In this study, high-performance LIC-ACE films were fabricated by an improved solution casting method that eliminates the need to press the LIC powder, greatly reducing the time-consuming manufacturing of pellets, eliminating the limitations imposed by the compressed surface, and further promoting the practical development of SSEs.

2. Material and methods

2.1. Preparation of LIC-ACE film

The anhydrous lithium chloride (LiCl, Innochem, 99.99 %) and anhydrous indium chloride ($InCl_3$, Sigma-Aldrich, 98 %) were dissolved in deionized water in the ratio of 3:1 (molar ratio) and then dried under vacuum at 100 °C until most of the water evaporated, and finally dried under vacuum at 200 °C for 6 h to obtain the final product LIC.

To prepare the electrolyte film 95 mg of LIC and 5 mg of ethyl cellulose (Sigma-Aldrich, 48.0 % (*w*/w) ethoxy basis and an average molecular weight of 100 g/mol) were added to 1 mL of anhydrous acetonitrile (CH_3CN, Sigma-Aldrich, 99.8 %), followed by slow magnetic stirring until powders are completely distributed in the solvent. The solution was slowly poured onto polymer filter membrane and vacuum filtered for 1 h to remove most of the acetonitrile. The microstructure of the filter membrane is shown in Fig. S1. Finally, the full dry sample is obtained by heating at 80 °C for 12 h under vacuum. At this point, the final sample, which we call LIC-ACE, is separated from the filter membrane with tweezers and has the form of a translucent film under light.

2.2. Characterization

The microscopic morphology and structure of the samples were observed by scanning electron microscopy and the elemental distribution was determined by energy dispersive spectroscopy. Ion conductivity, Electrochemical Impedance Spectroscopy (EIS), Cyclic Voltammetry (CV), charge/discharge tests were performed on a Biologic VSP Potentiation (France, Grenoble). The microstructure is visualized with a scanning electron microscope (SEM) **(**Zeiss Germany**)**. The crystal structure was determined by X-ray diffraction (XRD) using Rigaku MiniFlex X-ray diffractometer with Cu Kα radiation (λ = 1.54178 Å) (Japan, Tokyo). Information such as binding energy was collected using Al Ka source X-ray photoelectron spectroscopy (XPS) at 15 kV and 20 mA by PHI 5800 workstation (USA, Minneapolis). Stability under dry air was measured by thermogravimetric analysis (TGA) on Mettler Toledo Thermogravimetric Analyzer (Germany, Giessen). The specific surface area and adsorption/desorption curves were determined by ASAP 2020 PLUS BET analyzer using krypton at 77.39 K (USA).

2.3. Electrochemical performance measurement

The ionic conductivity was measured using LIC-ACE films peeled from the filter membrane by constructing SS (stainless steel)|LIC-ACE|SS cells and maintaining a pressure of 294 MPa during the test. Other electrochemical tests were performed by constructing ASSB, the cathode part is made by simply mixing LIC and NCM111 powder at a weight ratio of 3:7. At this time, the electronic conductivity of the composite cathode under high pressure has met the experimental requirements. Since we mainly focus on the research of SSE, we need to keep other components as simple as possible, and we do not add conductive agents. For the specific assembly process, 20 mg of the cathode composite material was placed on one side of the LIC-ACE film and then pressed with a pressure of 147 MPa. Finally, the Li foil is placed on the other side of the LIC-ACE film and pressed with a pressure of 98 MPa to obtain a sandwiched pellet for electrochemical testing. The test bench setup for ASSBs test is shown in Fig. S2. The activation energy (E_a) was computed by fitting the calculated diffusion coefficients to the standard Arrhenius form using the following relation:

$$D = D_0 exp\left(-\frac{E_a}{RT}\right)$$

3. Results and discussions

3.1. characterization of structural of LIC-ACE

LIC-ACE was prepared by casting LIC slurry on the surface of polymer filter by solution casting method. To evaluate the effect of different solvents on the result, we tested different solvents to their polarity, and the LIC-ACE, obtained using acetonitrile as the solvent, had the best overall performance. To obtain a structurally strong and flexible film, we added a small amount of amphiphilic binder such as ethyl cellulose (EC) to help the film formation [16,17]. It has been verified by many experiments with different amounts of EC added, it is finally determined that the addition of EC 5 % is the best. The smooth and porous polymer filter membrane was selected as the support for the LIC-ACE film.

The LIC-ACE appears under the light as a smooth milky film. By bending the filter membrane it can first be separated from the LIC-ACE, and then the complete LIC-ACE can be easily peeled off by using tweezers. Use punch to process LIC-ACE to get an edge-complete coin and after bending there are wrinkles, but the overall structure is still intact and there are no obvious breaks (Fig. 1a,b). We also tried to use traditional binders such as CMC and PVDF to prepare LIC film, but did not perform well, the film cracked after solvent removal and was not flexible (Fig. S3). This may be because the functional groups on the traditional binder can only form a stable structure with better cross-linking bonds with Li^+, while other ions such as In^{3+} cannot become good electron acceptors [18].

The LIC-ACE film appeared in SEM images as densely stacked nanorod clusters, with most of the rod-shaped monomers having a diameter of 2–6 μm and a length of about 50 μm (Fig. 1c). The monomers are connected by bridges, forming a relatively dense network structure that favors ion transport and provides structural strength (Fig. 1d). The longitudinal stacking between layers is relatively dense, but there are still some gaps and the densities can be further improved by applying a suitable pressure [19]. And the edge thickness is about 26 μm, reaching the thickness of commercial polymer separators (Fig. 1e). The results of EDS mapping show that elements such as C, O, In and Cl are evenly distributed. This shows that no material agglomeration occurred on the surface of LIC-ACE and the EC is well deposited in the LIC-ACE film providing mechanical stability and flexibility as the skeleton and does not participate in ion transfer (Fig. 1f, S4). The micropores, which serve as ion transport channels, are distributed over the entire surface, and pores are also present in the cross-section to prevent ion blockage (Fig. S5). In subsequent electrochemical tests, LIC-ACE will be used after high-pressure compaction, and the porosity of the film will be further reduced to avoid short circuits caused by direct contact between electrodes penetrating the film [20,21]. But the remaining micropores still allow Li^+ to pass evenly and rapidly through the electrolyte layer during charging and discharging [22–24]. And reduces the uneven deposition of lithium dendrites, which is one of the reasons for the good electrochemical performance [25]. The minimum thickness reachable with this method is around 10 μm however some mechanical constraints rise below 20 μm due to the reduced toughness that makes the cell

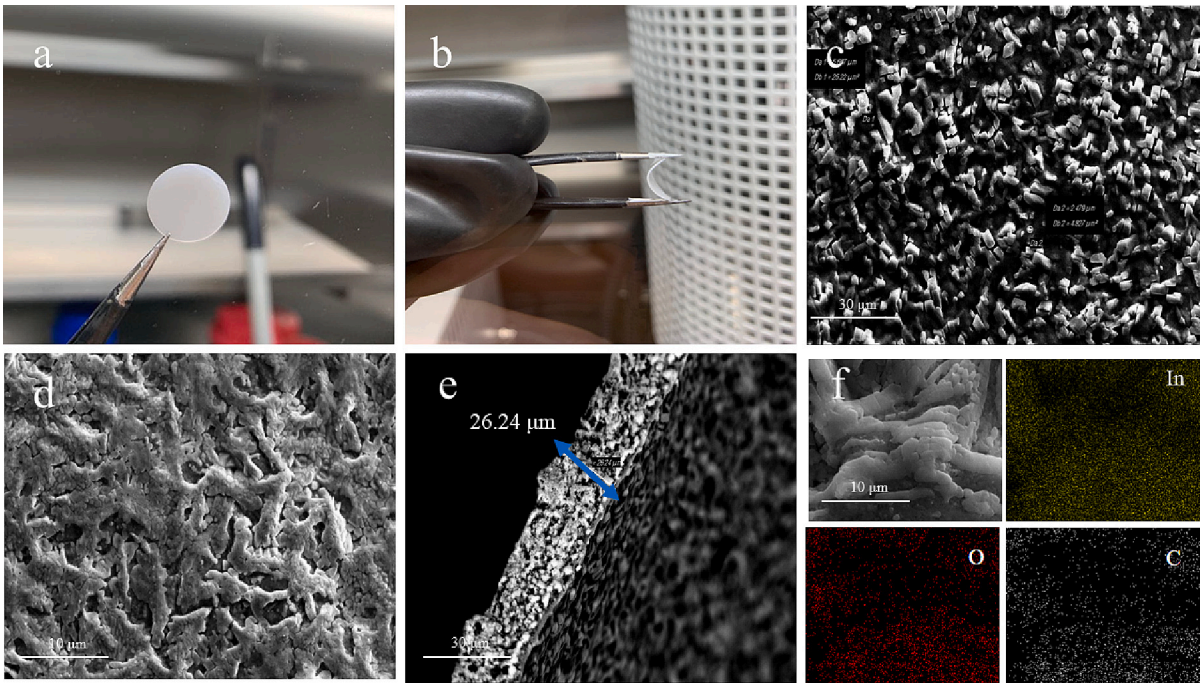

Fig. 1. (a) digital photo of LIC-ACE after cut. (b) Bending test of LIC-ACE. (c) SEM image of particle size of LIC-ACE. (d) SEM image of LIC-ACE structure. (e) SEM image of edge thickness of LIC-ACE. (f) EDS element mapping of LIC-ACE.

assembling particularly difficult. Since it is synthesized by the liquid phase method, the thickness of the LIC-ACE film can be easily controlled, which also facilitates subsequent electrochemical tests such as ionic conductivity.

3.2. Characterization of physicochemical properties of LIC-ACE

The XRD results of LIC-ACE are shown in Fig. 2a, and most of the sharp characteristic peaks, such as 13.9°, 27.4°, 33.6° and 48.4°, can be well indexed by Li_3InCl_6 (ICSD No. 89167, C2/m) with the monoclinic

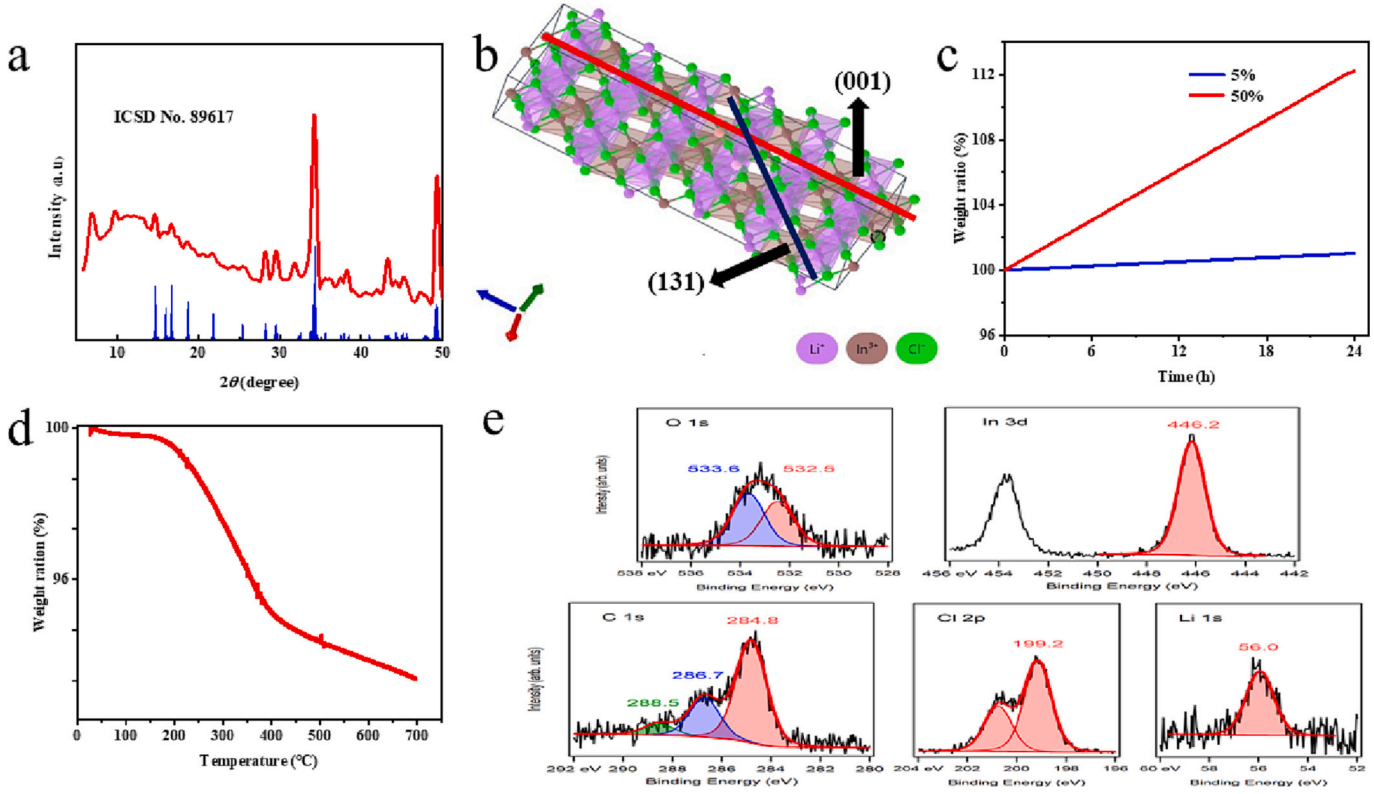

Fig. 2. (a) XRD pattern of LIC-ACE. (b) Typical crystal structure of LIC in the database. (c) Weight change plot of LIC-ACE at different humidity. (d) Thermogravimetric analysis curve of LIC-ACE. (e) O 1 s, In 3d, C 1 s, Li 1 s and Cl 2p, xps spectra of LIC-ACE.

rock-salt structure [26]. The typical crystal structure of Li_3InCl_6 is shown in Fig. 2b. Compared to the standard pattern, it is likely that the presence of residual tensile stress causes the anisotropic shrinkage of the lattice because EC has a high tensile strength (47–72 MPa), resulting in lattice distortion and larger interplanar spacing so that the peaks shift slightly to low angles. Among them, 13.9° and 33.6° represent the (001) and (131) planes of LIC respectively, and the peak intensity at 33.6° is much larger than that at 13.9°, indicating that the (131) plane is dominant. Because of the heterogeneity, when the (001) plane is the main orientation, it is difficult to arrange the single atoms in the unit cell to form a standard lattice, and Li^+ needs to overcome the interaction between the greater electrostatic force and the lattice [27]. Therefore, when the (131) plane is the main orientation, it can assist the transport of Li^+, which helps to compensate the decrease in ionic conductivity caused by the addition of EC. The peak around 5° can be retrieved as a small amount of residual LiCl, and the intensity of the two peaks between 27 and 31° exceeds expectations, which can be attributed to the superposition of LiCl and LIC [28,29]. The blunt peaks of low intensity at 9–12° and 19–22° can be retrieved as EC in LIC-ACE, indicating that EC exists in an amorphous state and is deposited as a skeleton throughout the sample [30]. It inhibits the excessive increase of crystallite size, improves the ordering of crystalline phases and reduces the strain [31]. The higher noise before 30° compared to the reference can also be explained by amorphous EC. The peak intensity of EC is low, does not cause the angle shift of the LIC peak, indicating good compatibility of LIC and EC in the case of acetonitrile as solvent. LIC-ACE presents a clear XRD pattern in total, and the good orientation of the crystal planes is maintained, proving that the solution casting method does not affect the structure and crystallinity of LIC when EC is added.

In SSEs, it is usually difficult to keep the properties stable in the air because of water absorption, oxidation, etc. The main problem plaguing HSSEs is strong hygroscopicity, so moisture resistance is also one of the important indicators for performance evaluation. LIC pellets show good stability in dry air, but after only a few minutes of exposure to higher humidity, they absorb moisture and become damp [30]. The slightest touch can cause disintegration of the structure and will gradually dissolve over time. We exposed LIC-ACE to air at 20 °C with 5 % and 50 % relative humidity at room temperature, and recorded the change in sample weight (Fig. 2c). After 24 h of exposure at 5 % relative humidity, the weight increase was very small, only about 0.5 %, so it can be assumed that the weight of the sample remained relatively stable. After 24 h of exposure at 50 % relative humidity, the weight increased by 12.2 %, but the shape of the sample did not change and the rigidity was maintained. Compared with LIC, which cannot exist stably in humid air, although LIC-ACE also absorbs a small amount of water, its hygroscopicity has been significantly weakened, especially in a relatively high-humidity environment. Moisturized LIC-ACE can also recover most of performance after proper heat treatment, which is similar to LIC [26]. The stability of LIC-ACE in 50 % relative humidity was also measured at higher temperatures. When the temperature was maintained at 50 °C, there was a slight decrease in sample weight (about 0.1 %) in the first few hours, which can be considered as the removal of a small amount of moisture absorbed during the operation. Afterwards, the sample weight remained unchanged until the end of the 24 h test (Fig. S6). This indicates that the stability of LIC-ACE in humid air can be maintained by heating, and the minimum maintenance temperature of 50 °C does not cause a large consumption of energy. The stability of LIC-ACE at high temperatures was verified by TGA, which was tested by heating the sample from room temperature to 700 °C at a rate of 5 °C min^{-1}. Until the temperature exceeds 200 °C, the weight of the sample begins to decrease, and EC begins to decompose, which proves that LIC-ACE has sufficient resistance to high temperature, and the solvent can be completely removed by heating at high temperature during the preparation process (Fig. 2d) [30]. LIC-ACE can remain intact at a temperature not exceeding 200 °C and has a certain resistance to air environments. Further, the trouble of moisture in the air can be eliminated by lower heating temperatures.

The details of the LIC-ACE binding energy change were further determined by XPS spectra (Fig. S7). The peaks of In $3d_{5/2}$ at 446.2 eV and In $3d_{3/2}$ at 453.8 eV, Cl 2p at 199.2 eV, O 1 s at 532.5 and 533.6 eV, are consistent with previous reported publications (Fig. 2e) [12,27,32,33]. The peak of Li 1 s shifted from the reference 56.6–56.2 to 56.0 eV, which can be attributed to the introduction of low electronegativity carbon after the addition of EC, resulting in a decrease in binding energy [34]. The peak of C 1s at 284.8 eV represents the C═C, which may come from the micro-cleavage of EC after heating [35,36]. The peaks at 286.7 and 288.5 eV can correspond to O1s, representing -COOH, -COH and -COC [37]. The XPS spectrum is consistent with the XRD analysis results, which proves the reliability of LIC-ACE.

The same EC showed a surface area of 6.279 $m^2 g^{-1}$ and a total pore volume of 0.1 $cm^3 g^{-1}$ in past tests [38]. According to the Kr adsorption/desorption isotherm test, The curve is similar to the type IV isotherm, and there is no saturated adsorption platform, indicating that the pore structure is irregular [39]. BET surface area of LIC-ACE containing 5 % EC is 1.6818 $m^2 g^{-1}$ and the total pore volume is 0.04 $cm^3 g^{-1}$ (Fig. S8). Since LIC is dispersed in the skeleton made of EC as a filler, the significant decrease in the BET surface area and total pore volume indicates that the pores of the sample have been almost uniformly filled by LIC [40]. It is worth noting that since EC only accounts for 5 % of the total mass of LIC-ACE, and the surface area of LIC is always less than 1 $m^2 g^{-1}$, but the final BET surface area still reaches 1.6818 $m^2 g^{-1}$, which also proves that the strategy is successful and the final sample still retains a relatively good surface area that can provide more contact surface for ion transfer.

3.3. Characterization of electrochemical performance of LIC-ACE

The ionic conductivity of LIC-ACE was first measured using the impedance spectrum of the symmetrical cell of SS|LIC|SS. The ionic conductivity values of LIC and LIC-ACE at room temperature are shown in Fig. 3a, where ionic conductivity at room temperature is 0.76 mS cm^{-1}. Equivalent circuit for EIS fitting show in Fig. S9. For comparison, the ionic conductivity of the LIC is 1.09 mS cm^{-1}. The ionic conductivity of LIC and LIC-ACE with different thicknesses is shown in Table S1, all measurements were carried out at steady state, and the average value was taken as the standard ionic conductivity. In other studies, the ionic conductivity of LIC is between 0.79 and 1.49 mS cm^{-1}, which is at a similar level to LIC-ACE [12,27,41,42]. The activation energy (E_a) of Li^+ migration reflects the level of the ion migration barrier and is calculated from the Arrhenius plot obtained from the Nyquist diagram at different temperatures, the LIC-ACE shows that the E_a is 0.289 eV (Fig. 3b). Due to the different details of the synthesis method, the activation energy of LIC is slightly different in studies, and the E_a is usually between 0.27 and 0.35 eV [12,43,44]. Although the activation energy increases after the addition of EC, but is still at the same level compared to the activation energy of LIC in other studies, so the Li^+ migration is almost unaffected on this side.

The symmetrical Li—Li cell without buffer layer was then constructed to verify the interfacial stability of the LIC-ACE/Li metal. At first, with the gradual increase of current density, the overpotential increases slowly from 0.2 mA cm^{-2} before reaching 0.8 mA cm^{-2}, so it can be considered that the critical current density is 0.8 mA cm^{-2} (Fig. 3c). Equivalent circuit for EIS fitting show in Fig. S10. The Li plating/stripping voltage profile show that the LIC-ACE cell could cycle stably for approximately 900 h, with the overpotential always increasing slowly and relatively smoothly without short-circuiting (Fig. 3d,e). During cycling, a stable interface gradually forms and the growth of lithium dendrites is limited to acceptable limits. However, after 900 h of cycling, the overpotential suddenly increases abnormally and after a few cycles the increase exceeds the sum of the previous 900 h, indicating a rapid deterioration in the stability of the interface. The test results of EIS at 0 h and 1000 h also prove this point, and the resistance at 1000 h is almost

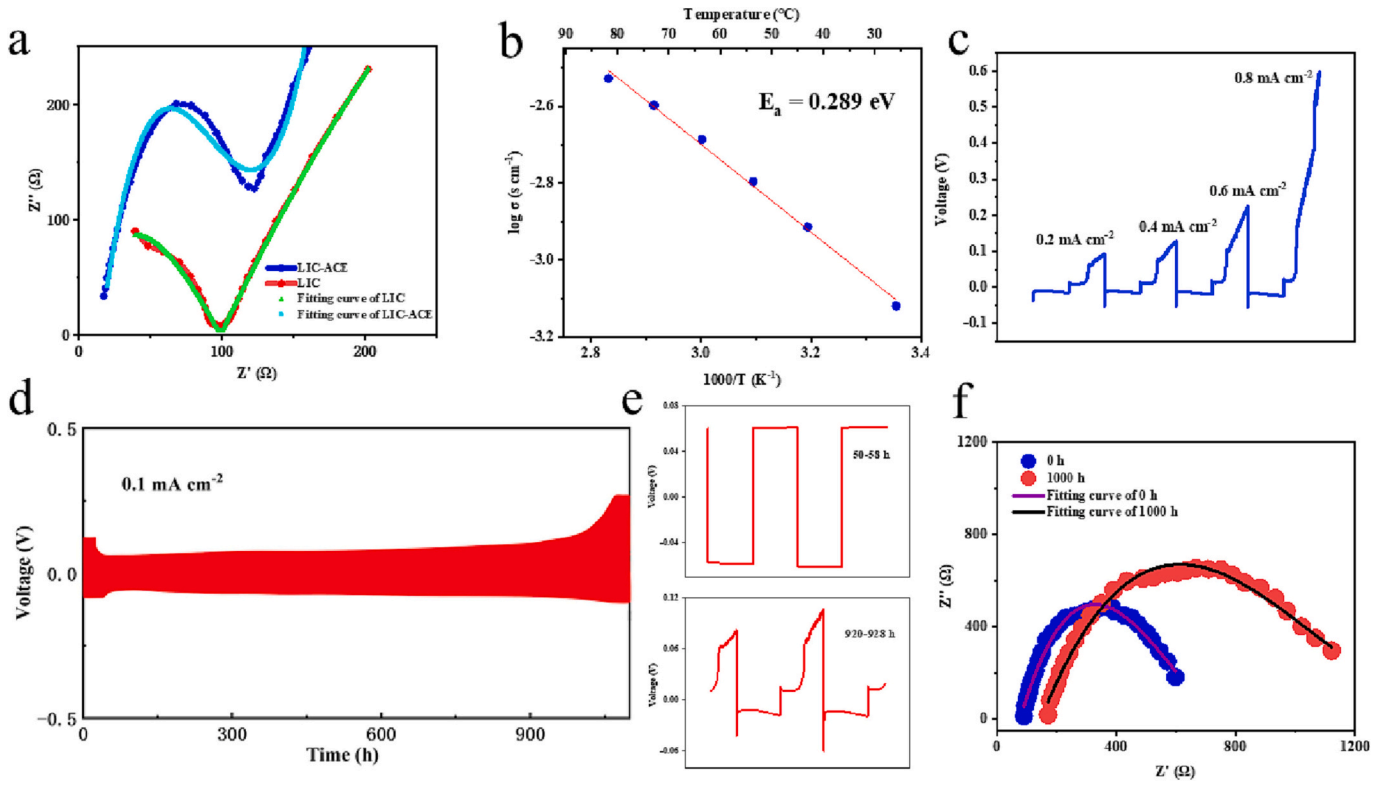

Fig. 3. (a) EIS and fitting plots of LIC-ACE and LIC at room temperature. (b) Arrhenius plot of LIC-ACE. (c) Rate performance of symmetric Li |LIC-ACE| Li cell. (d) Galvanostatic stripping/plating voltage profiles of symmetric Li |LIC-ACE| Li cell during 1100 h cycling. (e) Amplified voltage profiles at 50–54 and 920–924 h. (f) EIS plot of Li |LIC-ACE| Li cell at cycle 0 h and 1000 h.

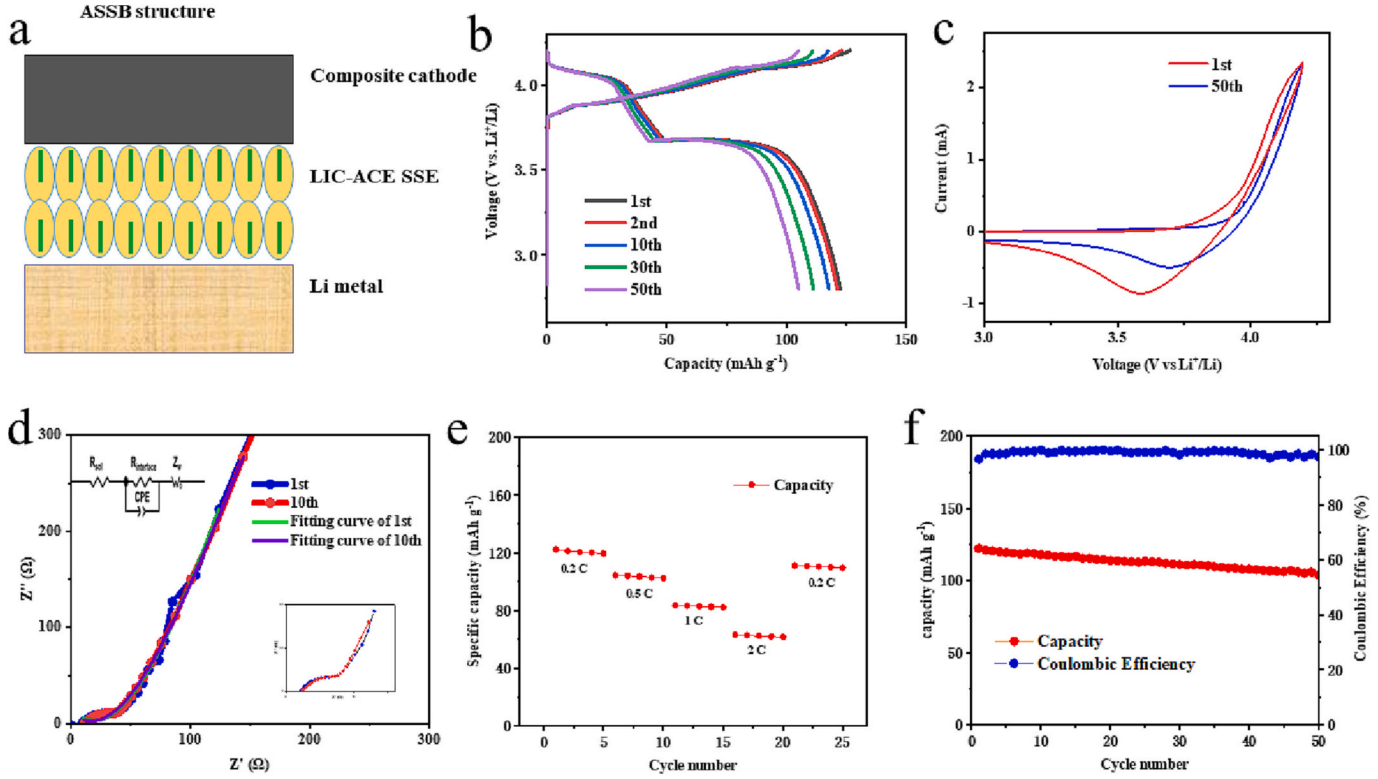

Fig. 4. (a) Schematic of LIC-ACE ASSB structure (b) Voltage profiles of LIC-ACE ASSB at different cycles. (c) CV curves at 1 mV s^{-1} after the first cycle and 50 cycles of LIC-ACE ASSB. (d) EIS, fitting plot and equivalent circuit of LIC-ACE ASSB after the first cycle and after 10 cycles. (e) rate capacity of LIC-ACE ASSB. (f) Cycling performance and CE of LIC-ACE ASSB.

doubled (Fig. 3f). LIC is thermodynamically unstable in direct contact with lithium metal, so previous works have often used sulfides as a buffer layer to improve the interfacial contact. We relied on a skeleton of EC to mitigate side reactions and short-circuiting caused by lithium dendrite penetration. Compared with the low performance of LIC symmetric cells in previous studies, the 900 h stability cycle proved this strategy to be effective [34,41].

The ASSB is assembled by NCM111-LIC mixed cathode, Li metal anode, and LIC-ACE. The initial discharge capacity of ASSB is 122.3 mAh g^{-1} at 0.2 C, under the same conditions, the profile of the charge-discharge curve does not change significantly with increasing number of cycles (Fig. 4b). The charge-discharge plateau caused by the reversible phase transition can be observed in both the charge-discharge curve and the CV curve (Fig. 4c). The trend of the CV curve measured after 50th is similar to the 1st, indicating the stable cycle performance of the overall electrode-electrolyte system. But the whole system changed a lot after 50th, which caused the oxidation peak and reduction peak in the CV curve to shift significantly compared with the 1st, and the integral area became smaller [45,46]. It also represents the capacity decrease, which is also consistent with the results of the charge/discharge process.

The EIS plot measured after 10 cycles still shows good performance compared to the first cycle, with only a slight change in the high-frequency range and instead a decrease in resistance in the low-frequency region, also indicating the structural stability of the LIC-ACE (Fig. 4d). It is tentatively concluded that the cathode is gradually activated during the charge/discharge process and wets itself with the LIC-ACE, resulting in better interfacial contact, so that the mass transfer resistance between the layers decreases. At various current rates of 0.2, 0.5, 1, and 2C, the discharge capacities of LIC-ACE ASSB are 122.2, 104.4, 83.6, and 63.3 mAh g^{-1}, respectively (Fig. 4e). After the 2 C cycle test, it was cycled again at 0.2C, and the discharge capacity returned to 111.2 mAh g^{-1}, illustrating the good capacity retention and rate performance of LIC-ACE ASSB. After 50 cycles, the capacity retention rate is 84.8 % and the coulombic efficiency (CE) of the first cycle is 94.5 %. After 5 cycles, CE can be stabilized at more than 99 %, and after 40 cycles, CE fluctuated but remains at 98 % (Fig. 4f). The high capacity and CE show good cycle stability, indicating that there are fewer side reactions during cycling.

4. Conclusion

In summary, this research has successfully demonstrated the feasibility of producing LIC-ACE films as SSEs through a modified solution casting method. The final sample was prepared by simply mixing LIC and EC in acetonitrile and then casting. The LIC-ACE film exhibited high ionic conductivity and good flexibility. LIC-ACE films have high ionic conductivity, and good flexibility and show good moisture resistance in dry air at various temperatures. The skeleton made of EC has good high-temperature performance, LIC are also uniformly filled in the skeleton. The electrochemical performance proves that it has good stability with electrode materials and good compatibility with Li metal, which can effectively reduce the occurrence of side reactions. LIC-ACE films can be synthesized on a large scale by the liquid phase method, saving the time needed to press the powder in the production step, which further promotes the practical development of SSE.

CRediT authorship contribution statement

The contribution of each author to the experimental sessions and to the redaction of the document were considered and the order of the authors was decided consequently in common agreement.

Declaration of competing interest

The authors declare that they have no known competing financial interests or personal relationships that could have appeared to influence the work reported in this paper.

Data availability

The data that has been used is confidential.

Acknowledgements

This research is funded by an industrial cooperation agreement with Phase Motion Control S.p.A. Italian company with siege in Genoa (Italy).

Appendix A. Supplementary data

Supplementary data to this article can be found online at https://doi.org/10.1016/j.est.2023.108244.

References

[1] J. Kagawa, Health effects of diesel exhaust emissions—a mixture of air pollutants of worldwide concern, Toxicology 181 (2002) 349–353.
[2] S. Foorginezhad, M. Mohseni-Dargah, Z. Falahati, et al., Sensing advancement towards safety assessment of hydrogen fuel cell vehicles[J], J. Power Sources 489 (2021), 229450.
[3] E. Figenbaum, M. Kolbenstvedt, B. Elvebakk, Electric vehicles–environmental, economic and practical aspects, in: As Seen by Current and Potential Users vol. 1329, 2014.
[4] L. Yiding, W. Wenwei, L. Cheng, et al., Multi-physics safety model based on structure damage for lithium-ion battery under mechanical abuse, J. Clean. Prod. 277 (2020), 124094.
[5] J. Hu, T. Liu, X. Wang, et al., Investigation on thermal runaway of 18,650 lithium ion battery under thermal abuse coupled with charging[J], J. Energy Storage 51 (2022), 104482.
[6] C. Li, Z.-y. Wang, Z.-j. He, et al., An advance review of solid-state battery: challenges, progress and prospects[J]. Sustainable, Mater. Technol. 29 (2021), e00297.
[7] Q. Zhao, S. Stalin, C.-Z. Zhao, et al., Designing solid-state electrolytes for safe, energy-dense batteries[J], Nat. Rev. Mater. 5 (3) (2020) 229–252.
[8] M.V. Reddy, C.M. Julien, A. Mauger, et al., Sulfide and oxide inorganic solid electrolytes for all-solid-state Li batteries: a review[J], Nanomaterials 10 (8) (2020) 1606.
[9] L. Yue, J. Ma, J. Zhang, et al., All solid-state polymer electrolytes for high-performance lithium ion batteries[J], Energy Storage Mater. 5 (2016) 139–164.
[10] L. Xu, J. Li, H. Shuai, et al., Recent advances of composite electrolytes for solid-state Li batteries[J], J. Energy Chem. 67 (2022) 524–548.
[11] T. Asano, A. Sakai, S. Ouchi, et al., Solid halide electrolytes with high lithium-ion conductivity for application in 4 V class bulk-type all-solid-state batteries[J], Adv. Mater. 30 (44) (2018) 1803075.
[12] X. Li, J. Liang, J. Luo, et al., Air-stable Li 3 InCl 6 electrolyte with high voltage compatibility for all-solid-state batteries[J], Energy Environ. Sci. 12 (9) (2019) 2665–2671.
[13] J. Xu, L. Liu, N. Yao, et al., Liquid-involved synthesis and processing of sulfide-based solid electrolytes, electrodes, and all-solid-state batteries[J], Mater. Today Nano. 8 (2019), 100048.
[14] C. Wang, J. Liang, J. Luo, et al., A universal wet-chemistry synthesis of solid-state halide electrolytes for all-solid-state lithium-metal batteries[J], Sci. Adv. 7 (37) (2021), eabh1896.
[15] M. Kotobuki, K. Kanamura, Y. Sato, et al., Electrochemical properties of Li7La3Zr2O12 solid electrolyte prepared in argon atmosphere[J], J. Power Sources 199 (2012) 346–349.
[16] X. Wu, L. Zhang, X. Zhang, et al., Ethyl cellulose nanodispersions as stabilizers for oil in water Pickering emulsions[J], Sci. Rep. 7 (1) (2017) 1–10.
[17] D. Cao, Q. Li, X. Sun, et al., Amphipathic binder integrating ultrathin and highly ion-conductive sulfide membrane for cell-level high-energy-density all-solid-state batteries[J], Adv. Mater. 33 (52) (2021) 2105505.
[18] F.J. Simon, M. Hanauer, F.H. Richter, et al., Interphase formation of PEO20: LiTFSI–Li6PS5Cl composite electrolytes with lithium metal[J], ACS Appl. Mater. Interfaces 12 (10) (2020) 11713–11723.
[19] Q. Duan, S. Wang, Q. Wang, et al., Simultaneous improvement on strength, modulus, and elongation of carbon nanotube films functionalized by hyperbranched polymers[J], ACS Appl. Mater. Interfaces 11 (39) (2019) 36278–36285.
[20] H. Shen, E. Yi, S. Heywood, et al., Scalable Freeze-tape-casting Fabrication and Pore Structure Analysis of 3D LLZO Solid-state Electrolytes 12(3), 2019, pp. 3494–3501.
[21] C. Lee, S.Y. Han, J.A. Lewis, et al., Stack Pressure Measurements to Probe the Evolution of the Lithium–solid-state Electrolyte Interface 6(9), 2021, pp. 3261–3269.
[22] F. Zhu, M.S. Islam, L. Zhou, et al., Single-atom-layer Traps in a Solid Electrolyte for Lithium Batteries 11(1), 2020, p. 1828.

[23] T. Hamann, L. Zhang, Y. Gong, et al., The effects of constriction factor and geometric tortuosity on Li-ion transport in porous solid-state Li-ion electrolytes[J], Adv. Funct. Mater. 30 (14) (2020) 1910362.
[24] X.X. Wang, X.W. Chi, M.L. Li, et al., Metal–organic frameworks derived electrolytes build multiple wetting interfaces for integrated solid-state lithium–oxygen battery, Adv. Funct. Mater. (2022) 2113235.
[25] H. Zhao, N. Deng, W. Kang, et al., Highly multiscale structural Poly (vinylidene fluoridehexafluoropropylene)/poly-m-phenyleneisophthalamide separator with enhanced interface compatibility and uniform lithium-ion flux distribution for dendrite-proof lithium-metal batteries, Energy Storage Mater. 26 (2020) 334–348.
[26] X. Li, J. Liang, N. Chen, et al., Water-mediated synthesis of a superionic halide solid electrolyte[J], Angew. Chem. 131 (46) (2019) 16579–16584.
[27] X. Luo, D. Cai, X. Wang, et al., A novel ethanol-mediated synthesis of superionic halide electrolytes for high-voltage all-solid-state lithium–metal batteries, ACS Appl. Mater. Interfaces 14 (26) (2022) 29844–29855.
[28] I. Elashmawi, Effect of LiCl filler on the structure and morphology of PVDF films [J], Mater. Chem. Phys. 107 (1) (2008) 96–100.
[29] N. Li, X. Li, T. Zhang, et al., Host–guest composite materials of LiCl/NaY with wide range of humidity sensitivity[J], Mater. Lett. 58 (10) (2004) 1535–1539.
[30] M.K. Trivedi, A. Branton, D. Trivedi, et al., Characterization of physicochemical and thermal properties of biofield treated ethyl cellulose and methyl cellulose[J], Int. J. Biomed. Mater. Res. 3 (6) (2015) 83–91.
[31] K.K. Khichar, S.B. Dangi, V. Dhayal, et al., Structural, optical, and surface morphological studies of ethyl cellulose/graphene oxide nanocomposites[J], Polym. Compos. 41 (7) (2020) 2792–2802.
[32] S. Deng, M. Jiang, A. Rao, et al., Fast-charging halide-based all-solid-state batteries by manipulation of current collector interface[J], Adv. Funct. Mater. (2022) 2200767.
[33] D. Briggs, G. Beamson, XPS studies of the oxygen 1s and 2s levels in a wide range of functional polymers[J], Anal. Chem. 65 (11) (1993) 1517–1523.
[34] X. Chen, Z. Jia, H. Lv, et al., Improved stability against moisture and lithium metal by doping F into Li3InCl6[J], J. Power Sources 545 (2022), 231939.
[35] N.M. Brown, J.A. Hewitt, B.J. Meenan, X-ray photoelectron spectroscopy and infrared studies of X-ray-induced beam damage of cellulose, ethyl cellulose and ethylhydroxyethyl cellulose[J], Surf. Interface Anal. 18 (3) (1992) 199–209.
[36] J. Shi, W. Liu, X. Jiang, et al., Preparation of cellulose nanocrystal from tobacco-stem and its application in ethyl cellulose film as a reinforcing agent[J], Cellulose 27 (3) (2020) 1393–1406.
[37] D.V. Sivkov, O.V. Petrova, S.V. Nekipelov, et al., Quantitative characterization of oxygen-containing groups on the surface of carbon materials: XPS and NEXAFS study[J], Appl. Sci. 12 (15) (2022) 7744.
[38] E.S. Pouya, H. Fatoorehchi, M. Foroughi-Dahr, Batch removal of Pb (II) ions from aqueous medium using gamma-Al2O3 nanoparticles/ethyl cellulose adsorbent fabricated via electrospinning method: an equilibrium isotherm and characterization study[J], Pol. J. Chem. Technol. 20 (2) (2018).
[39] M. Naderi, Surface area: Brunauer–Emmett–Teller (BET), in: Progress in Filtration and Separation, Elsevier, 2015, pp. 585–608.
[40] Z. Wang, R. Tan, H. Wang, et al., A metal–organic-framework-based electrolyte with nanowetted interfaces for high-energy-density solid-state lithium battery[J], Adv. Mater. 30 (2) (2018) 1704436.
[41] Z. Deng, Z. Jin, D. Chen, et al., Bilayer halide electrolytes for all-inorganic solid-state Lithium-metal batteries with excellent interfacial compatibility[J], ACS Appl. Mater. Interfaces 14 (43) (2022) 48619–48626.
[42] P. Molaiyan, S.E. Mailhiot, K. Voges, et al., Investigation of the structure and ionic conductivity of a Li3InCl6 modified by dry room annealing for solid-state Li-ion battery applications[J], Mater. Des. 227 (2023), 111690.
[43] F. Hussain, J. Zhu, H. Xia, et al., Theoretical insights on the comparison of Li-ion conductivity in halide superionic conductors Li3MCl6, Li2M2/3Cl4, and LiMCl4 (M = Y, Sc, Al, and Sm)[J], J. Phys. Chem. C 126 (31) (2022) 13105–13113.
[44] W. Li, J. Liang, M. Li, et al., Unraveling the origin of moisture stability of halide solid-state electrolytes by in situ and operando synchrotron X-ray analytical techniques[J], Chem. Mater. 32 (16) (2020) 7019–7027.
[45] X. Pu, D. Zhao, C. Fu, et al., Understanding and calibration of charge storage mechanism in cyclic voltammetry curves[J], Angew. Chem. Int. Ed. 60 (39) (2021) 21310–21318.
[46] T. Kim, W. Choi, H.-C. Shin, et al., Applications of voltammetry in lithium ion battery research[J], J. Electrochem. Sci. Technol. 11 (1) (2020) 14–25.